JOURNAL OF BONE AND MINERAL RESEARCH
Volume 23, Number 6, 2008
Published online on December 17, 2007; doi: 10.1359/JBMR.071213

Enzyme Replacement Therapy for Murine Hypophosphatasia*

José Luis Millán,[1] Sonoko Narisawa,[1] Isabelle Lemire,[2] Thomas P Loisel,[2] Guy Boileau,[3] Pierre Leonard,[2] Svetlana Gramatikova,[1] Robert Terkeltaub,[4] Nancy Pleshko Camacho,[5] Marc D McKee,[6] Philippe Crine,[2] and Michael P Whyte[7]

ABSTRACT:

Introduction: Hypophosphatasia (HPP) is the inborn error of metabolism that features rickets or osteomalacia caused by loss-of-function mutation(s) within the gene that encodes the tissue-nonspecific isozyme of alkaline phosphatase (TNALP). Consequently, natural substrates for this ectoenzyme accumulate extracellulary including inorganic pyrophosphate (PP_i), an inhibitor of mineralization, and pyridoxal 5′-phosphate (PLP), a co-factor form of vitamin B_6. Babies with the infantile form of HPP often die with severe rickets and sometimes hypercalcemia and vitamin B_6-dependent seizures. There is no established medical treatment.
Materials and Methods: Human TNALP was bioengineered with the C terminus extended by the Fc region of human IgG for one-step purification and a deca-aspartate sequence (D_{10}) for targeting to mineralizing tissue (sALP-FcD_{10}). TNALP-null mice (*Akp2*$^{-/-}$), an excellent model for infantile HPP, were treated from birth using sALP-FcD_{10}. Short-term and long-term efficacy studies consisted of once daily subcutaneous injections of 1, 2, or 8.2 mg/kg sALP-FcD_{10} for 15, 19, and 15 or 52 days, respectively. We assessed survival and growth rates, circulating levels of sALP-FcD_{10} activity, calcium, PP_i, and pyridoxal, as well as skeletal and dental manifestations using radiography, μCT, and histomorphometry.
Results: *Akp2*$^{-/-}$ mice receiving high-dose sALP-FcD_{10} grew normally and appeared well without skeletal or dental disease or epilepsy. Plasma calcium, PP_i, and pyridoxal concentrations remained in their normal ranges. We found no evidence of significant skeletal or dental disease.
Conclusions: Enzyme replacement using a bone-targeted, recombinant form of human TNALP prevents infantile HPP in *Akp2*$^{-/-}$ mice.
J Bone Miner Res 2008;23:777–787. Published online on December 17, 2007; doi: 10.1359/JBMR.071213

Key words: alkaline phosphatase, calcification, epilepsy, osteomalacia, rickets

INTRODUCTION

HYPOPHOSPHATASIA (HPP) IS a rare, heritable form of rickets or osteomalacia[1–4] with an incidence as great as 1 per 2500 births in Canadian Mennonites.[5] This "inborn error of metabolism" is caused by loss-of-function mutation(s) in the gene (*ALPL*) that encodes the tissue-nonspecific isozyme of alkaline phosphatase (TNALP; a.k.a. liver/bone/kidney type ALP).[6–10] The biochemical hallmark of HPP is subnormal ALP activity in serum (hypophosphatasemia), leading to elevated blood or urine levels of three phosphocompounds: phosphoethanolamine (PEA), inorganic pyrophosphate (PP_i), and pyridoxal 5′-phosphate (PLP).[4]

HPP features a remarkable range of severity spanning (most severe to mildest) perinatal, infantile, childhood, and adult forms classified according to age at diagnosis with skeletal disease.[2,4] There may be absence of bone mineralization in utero with stillbirth or spontaneous fractures presenting during adult life. Odonto-HPP causes premature loss of deciduous teeth without evidence of skeletal disease.[4]

In infantile HPP, diagnosed before 6 mo of age, postnatal development seems normal until onset of poor feeding, in-

*Presented in part at the 5th International Alkaline Phosphatase Symposium, May 16–19, 2007, Huningue, France; the 17th Scientific Meeting, International Bone and Mineral Society, June 24–29, 2007, Montreal, Canada; and the 29th Annual Meeting of the American Society for Bone and Mineral Research, September 16–19, 2007, Honolulu, Hawaii, USA.

Drs Lemire, Loisel, Leonard, and Crine are employees of Enobia Pharma. Drs Millán, McKee, Boileau, and Whyte are consultants for Enobia Pharma. All other authors state that they have no conflicts of interest.

[1]Burnham Institute for Medical Research, La Jolla, California, USA; [2]Enobia Pharma, Montreal, Quebec, Canada; [3]University of Montreal, Montreal, Quebec, Canada; [4]VAMC/UCSD, San Diego, California, USA; [5]The Hospital for Special Surgery, New York, New York, USA; [6]McGill University, Montreal, Quebec, Canada; [7]Shriners Hospitals for Children and Washington University, St Louis, Missouri, USA.

adequate weight gain, and the appearance of rickets. Radiographs show impaired skeletal mineralization leading to rib fractures and chest deformity. Consequently, there is hypercalcemia[3,4] and respiratory failure. TNALP-null mice (*Akp2*$^{-/-}$) phenocopy infantile HPP extremely well.[11–13] They are born with a normally mineralized skeleton but develop radiographically apparent rickets at ~6 days of age and die between day 12 and 16, suffering severe skeletal hypomineralization and epileptic seizures attributable to disturbances in PLP (vitamin B_6) metabolism.[11,14]

In the healthy skeleton, TNALP is an ectoenzyme present on the surface of the plasma membrane of osteoblasts and chondrocytes, including on the membrane of their shed matrix vesicles (MVs)[15,16] where the enzyme is particularly enriched.[17] Electron microscopy showed that TNALP-deficient MVs from severely affected HPP patients and *Akp2*$^{-/-}$ mice contain hydroxyapatite crystals, but extravesicular crystal propagation is compromised.[18,19] The resulting defect in skeletogenesis is attributed to the extracellular accumulation of PP_i, a potent inhibitor of mineralization.[3,4,20–24] The biochemical pathway involved and the consequences of PEA elevation in HPP patients or *Akp2*$^{-/-}$ mice remain uncertain.[4,10]

There is no established medical therapy for HPP.[4] Case reports of attempted enzyme replacement therapy (EzRT) using intravenous infusions of ALP-rich plasma from Paget's bone disease patients, purified human liver ALP, or purified human placental ALP document failure to rescue affected infants.[25–28] It seems that ALP activity must be increased not in the circulation, but in the HPP skeleton itself. This hypothesis is supported by the favorable outcomes of two girls with infantile HPP after attempts to transplant mesenchyme-derived cells, where perhaps small numbers of TNALP-containing osteoblasts and chondrocytes were introduced throughout the skeleton.[29,30]

Here, we assessed an EzRT strategy for HPP using the *Akp2*$^{-/-}$ mouse model of the infantile form of the disease given recombinant human TNALP optimized for delivery to bone.

MATERIALS AND METHODS

Bioengineering and expression of recombinant sALP-FcD$_{10}$

The sALP-FcD$_{10}$ protein contains recombinant human soluble TNALP (sALP), the constant region of human IgG1 Fc domain (Fc), and a deca-aspartate motif (D_{10}). The cDNA encoding the fusion protein was inserted into the pIRES vector (Clontech, San Diego, CA, USA) in the first multiple cloning site located upstream of the IRES using *Nhe*I and *Bam*HI endonuclease restriction sites. The dihydrofolate reductase (DHFR) gene was inserted into the second multiple cloning site located downstream of the IRES using *Sma*I and *Xba*I endonuclease restriction sites. The resulting vector was transfected into Chinese Hamster Ovary (CHO-DG44) cells lacking both DHFR gene alleles[31] (obtained from Dr Lawrence A Chasin, Columbia University, New York, NY, USA) using the Lipofectamine transfection kit (Invitrogen, San Diego, CA, USA). Two days after transfection, media were changed, and the cells were maintained in a nucleotide-free medium (IMDM supplemented with 5% dialyzed FBS) for 15 days to isolate stable transfectants for plaque cloning. Cells from three clones growing in the nucleotide-free medium were pooled and further cultivated in media (IMDM + 5% dialyzed FBS) containing increasing concentrations of methotrexate (MTX). Cultures resistant to 50 nM MTX were further expanded in Cellstacks (Corning) containing IMDM medium supplemented with 5% FBS. On reaching confluency, the cell layer was rinsed with PBS, and the cells were incubated for 3 additional days with IMDM containing 3.5 mM sodium butyrate to increase protein expression. At the end of the culture, the concentration of sALP-FcD$_{10}$ in the spent medium was 3.5 mg/liter as assessed by TNALP enzymatic activity. Culture supernatant was concentrated and dialyzed against PBS using tangential flow filtration and loaded on to Protein A-Sepharose columns (Hi-Trap 5 ml; GE Health Care) equilibrated with PBS. Bound proteins were eluted with 100 mM citrate, pH 4.0 buffer. Collected fractions were immediately adjusted to pH 7.5 with 1 M Tris pH 9.0. Fractions containing most of the eluted material were dialyzed against 150 mM NaCl, 25 mM sodium PO_4, pH 7.4, buffer containing 0.1 mM $MgCl_2$ and 20 μM $ZnCl_2$ and filtered through a 0.22-μm (Millex-GP; Millipore) membrane under sterile conditions. The overall yield of the purification procedure was 50%, with purity surpassing 95% as assessed by Sypro ruby stained SDS-PAGE. Purified sALP-FcD$_{10}$ preparations were stored at 4°C and remained stable for several months.

Labeling of sALP-FcD$_{10}$

An aliquot containing 4 mg of sALP-FcD$_{10}$ was iodinated with IODO-BEADS (Pierce) according to the manufacturer's instructions. The final iodination mix contained two IODO-BEADS in a total volume of 2.5 ml of iodination buffer (150 mM NaCl, 25 mM Na phosphate, pH 7.4). Reaction was initiated by the addition of 1 mCi Na[^{125}I] and left to proceed at room temperature for 5 min before quenching with 25 μl 1.85×10^{-3} M NaI and desalting on a PD-10 column (Pharmacia). Total specific radioactivity of the labeled enzyme was ~50,000 dpm/μg. The specific activity of the enzyme after labeling was at least 95% that of the unlabeled enzyme.

Binding of sALP-FcD$_{10}$ to hydroxyapatite

sALP-FcD$_{10}$ and bovine kidney TNALP were compared in a reconstituted mineral-binding assay. For this experiment, hydroxyapatite ceramic beads were first solubilized in 1 M HCl, and the mineral was precipitated by bringing back the solution to pH 7.4 with 10 N NaOH. Binding to this reconstituted mineral was studied by incubating aliquots of the mineral suspension containing 750 μg of mineral with 5 μg of protein in 100 μl of 150 mM NaCl and 80 mM sodium phosphate, pH 7.4, buffer. The samples were kept at 21 ± 2°C for 30 min on a rotating wheel. Mineral was spun down by low-speed centrifugation, and total enzymatic activity, recovered in both the mineral pellet and the supernatant, was measured.

Mouse model of infantile HPP

The *Akp2*$^{-/-}$ mice, created by insertion of the Neo cassette into exon 6 of the mouse TNALP gene (*Akp2*) through homologous recombination, functionally inactivate the *Akp2* gene resulting in no detectable TNALP mRNA or protein.[12] Phenotypically, *Akp2*$^{-/-}$ knockout mice closely mimic infantile HPP.[13] Like HPP patients, *Akp2*$^{-/-}$ mice have global deficiency of TNALP activity, endogenous accumulation of the ALP substrates PP_i, PLP, and PEA, and postnatally manifest an acquired defect in mineralization of skeletal matrix leading to rickets or osteomalacia.[13] They have stunted growth and develop radiographically and histologically apparent rickets together with epileptic seizures and apnea and die between postnatal days 10 and 12.[11–14] In our current studies, we also documented hypercalcemia, which occurs in some severely affected HPP patients we believe from failure of mineral uptake by the skeleton together with skeletal demineralization.[4] Pyridoxine supplementation briefly suppresses the seizures in these mice and extends their lifespan, but only until postnatal days 18–22. Therefore, all animals (breeders, nursing mothers and their pups, and weanlings) were given free access to modified laboratory rodent diet 5001 containing increased levels (325 ppm) of pyridoxine. To identify *Akp2*$^{-/-}$ homozygotes at day 0 (date of birth), we used 0.5 μl of whole blood obtained at the time of toe clipping and measured serum ALP activity in a total reaction volume of 25 μl, velocity of 30 min at OD 405, with 10 mM *p*-nitrophenolphosphate (pNPP). The genotype of the animals was confirmed by PCR and/or Southern blotting using tail DNA obtained at the time of tissue collection.

ALP assay

Nonfasting blood was collected by cardiac puncture into lithium heparin tubes (CBD365958; VWR), put on wet ice for a maximum of 20 min, and centrifuged at 2500*g* for 10 min at room temperature. At least 15 μl of plasma was transferred into 0.5-ml tubes (72.699; Sarstedt), frozen in liquid N_2, and kept at −80°C until assayed for ALP activity and PP_i concentrations. Any remaining plasma was pooled with the 15-μl aliquot, frozen in liquid N_2, and kept at −80°C. Levels of sALP-FcD_{10} in plasma were quantified using a colorimetric assay for ALP activity where absorbance of released *p*-nitrophenol is proportional to the reaction products. The reaction occurred in 100 μl of ALP buffer (20 mM Bis Tris Propane [HCl], pH 9, 50 mM NaCl, 0.5 mM $MgCl_2$, and 50 μM $ZnCl_2$) containing 10 μl of diluted plasma and 1 mM pNPP. The latter compound was added last to initiate the reaction. Absorbance was recorded at 405 nm every 45 s over 20 min using a spectrophotometric plate reader. sALP-FcD_{10} catalytic activity, expressed as an initial rate, was assessed by fitting the steepest slope for eight sequential values. Standards were prepared with varying concentrations of sALP-FcD_{10}, and ALP activity was determined as above. The standard curve was generated by plotting log of the initial rate as a function of the log of the standard concentrations. sALP-FcD_{10} concentration in the different plasma samples was read from the standard curve using their respective ALP absorbance. Activity measures were transformed into concentrations of sALP-FcD_{10} using a calibration curve obtained by plotting the activity of known concentrations of purified recombinant enzyme.

PP_i assay

Circulating levels of PP_i were measured using plasma and differential adsorption on activated charcoal of UDP-D-[6-^{3}H]glucose (Amersham Pharmacia) with the reaction product of 6-phospho[6-^{3}H]gluconate, as previously described.[32]

Vitamin B_6 assays

Pyridoxal 5′-phosphate (PLP) and pyridoxal (PL) concentrations in plasma were measured by HPLC as described.[33]

Plasma calcium

Plasma total calcium was measured using the orthocresolphthalein complexone method.[34]

Skeletal and dental tissue preparation and morphological analysis

After anesthesia with Avertin and blood collection using exsanguination, soft tissue was dissected away, and bones were fixed in 4% paraformaldehyde in PBS for 3 days and washed in a series of sucrose (10%, 15%, 20%)/PBS mixtures containing 1 mM $MgCl_2$ and 1 mM $CaCl_2$ at 4°C. Bones embedded in optimal cutting temperature (OCT) compound were sectioned using a Leica CM1800 cryostat. Sections (~9 mm) were vacuum dried for 1 h, immediately washed in PBS, and transferred to freshly prepared staining mixture of Naphthol AS-MX phosphate disodium salt and Fast Violet B salt (Sigma, St Louis, MO, USA) as described.[35] Methyl green (0.0001%) served as counterstain.

Proximal tibias were separated using a slow-speed saw. The specimens were dehydrated through a series of ascending ethanol solutions, cleared with xylene, infiltrated with methylmethacrylate, and embedded in methylmethacrylate/catalyst. Frontal sections, through the middle of the tibia, were obtained using a rotary microtome (Model RM2165; Leica Microsystems, Bannockburn, IL, USA). One 4-μm section was stained with Goldner's trichrome stain.

Mandibles from 16-day-old mice were immersion-fixed overnight in sodium cacodylate-buffered aldehyde solution and cut into segments containing the first molar, the underlying incisor, and the surrounding alveolar bone. Samples were dehydrated through a graded ethanol series and infiltrated with either acrylic (LR White) or epoxy (Epon 812) resin, followed by polymerization of the tissue-containing resin blocks at 55°C for 2 days. Thin sections (1 μm) were cut on an ultramicrotome using a diamond knife, and glass slide-mounted sections were stained for mineral using 1% silver nitrate (von Kossa staining, black) and counterstained with 1% toluidine blue. Frontal sections through the mandibles (at the same level of the most mesial root of the first molar) provided longitudinally sectioned molar and cross-sectioned incisor for comparative histological analyses.

X-ray analysis

Radiographic images were obtained with a Faxitron MX-20 DC4 (Faxitron X-ray Corp., Wheeling, IL, USA) using an energy of 26 kV and an exposure time of 10 s.

μCT analysis

Formalin-fixed lumbar vertebrae, femora, and calvaria were analyzed for bone architecture using the MS-8 system (GE Healthcare, London, Ontario, Canada) and isotropic voxel resolution of 18 μm. In each scan, a calibration phantom including air, water, and a mineral standard material (SB3; Gammex RMI) enabled calibration and conversion of X-ray attenuation such that mineral density was proportional to grayscale values in Hounsfield units. Digital reconstruction of ray projection to CT volume data was accomplished with a modified Parker algorithm. After reconstruction, images were "thresholded" automatically to distinguish bone voxels using a built-in algorithm of the GE-supplied MicroView software. BMD (mg/ml), trabecular thickness (Tb.Th.; mm), and the number of trabeculae (Tb.N.; mm^{-3}) were measured in the trabecular bone region of the centrum (body) of the L_2 vertebra. The region of interest (ROI) was defined as an elliptical cylinder with dimensions $0.45 \times 1.0 \times 0.9$ mm. Care was taken to exclude cortical bone from these measurements. The trabecular bone volume fraction (BVF) was calculated as the number of bone voxels divided by the total number of voxels (BV/TV) within the ROI. BMD was also measured in the parietal region of the calvaria with the ROI defined as a cube that enclosed a 3-mm-wide segment of the parietal bone. Cortical bone thickness and area were measured in the femur with the ROI defined as a 1.0-mm-long segment at the mid-diaphysis.

Pharmacokinetic analysis

The WinNonlin 5.2 software package (Pharsight Corp., Mountain View, CA, USA) was used to predict the circulating blood levels of sALP-FcD_{10} after repeated injections.

Statistical analysis

Nonparametric analyses were preferred for all parameters because of the small sample sizes. The log-rank test was used to compare survival curves. χ^2 was performed to test the distribution of radiographic severity between treatment with sALP-FcD_{10} and vehicle. The Kruskal-Wallis test was used to compare changes in body weights between the three groups of mice at each day. The Wilcoxon two-sample rank sum test or the Mann-Whitney rank sum test was performed to compare the two sets of treatments.

RESULTS

Production and characterization of sALP-FcD_{10}

To facilitate the expression and purification of recombinant human TNALP, we removed its hydrophobic C-terminal sequence that specifies GPI-anchor attachment, thereby creating a soluble secreted enzyme,[36] and also extended the coding sequence of its ectodomain with the Fc region of human IgG (γ1 form). This allowed rapid purification of the recombinant enzyme using protein A chromatography. Furthermore, to target the recombinant TNALP to bone tissue, a mineral-binding deca-aspartate (D_{10}) sequence[37] was added as an extension to the C terminus of both Fc regions. The fraction of sALP-FcD_{10} protein purified on Protein-A Sepharose was analyzed using SDS-PAGE under reducing conditions, where it migrated as a broad band with an apparent molecular mass of ~90,000 Da. Peptide N-glycosidase F (PNGAse F) digestion reduced the apparent molecular mass to ~80,000 Da, which closely approximates the calculated mass of 80,500 Da for the nonglycosylated sALP-FcD_{10} monomer. Using SDS-PAGE under nonreducing conditions, the apparent molecular mass of sALP-FcD_{10} was ~200,000 Da (Fig. 1A), consistent with a dimer, as in native, unaltered, TNALP.[10] This homodimeric form of TNALP most likely results from two disulfide bridges in the hinge domain of two monomeric Fc regions. The molecular mass of sALP-FcD_{10} under native conditions was ~370 kDa, suggesting a tetrameric form for the native sALP-FcD_{10} recombinant enzyme produced in CHO cells (Fig. 1B).

The affinity of the purified sALP-FcD_{10} protein for hydroxyapatite mineral was contrasted to that of soluble TNALP purified from bovine kidney. Total activity was the sum of the enzymatic activity recovered in the free and bound fractions and was found to be 84% and 96% of enzymatic activity introduced in each set of assays for the bovine and sALP-FcD_{10} forms of enzyme, respectively. Results are the average of two bindings. The sALP-FcD_{10} bound 32-fold more efficiently to reconstituted hydroxyapatite than did the bovine kidney TNALP. Furthermore, most of the recombinant sALP-FcD_{10} protein introduced in the assay was accounted for by summing up the enzymatic activity recovered in the bound and nonbound fractions. This indicated that binding of sALP-FcD_{10} to mineral does not significantly alter its enzymatic activity.

Pharmacokinetic properties of sALP-FcD_{10}

Next, we determined the pharmacokinetics (PK) and tissue distribution of sALP-FcD_{10} in adult and newborn mice comparing different routes of administration. First, we injected a single intravenous bolus of 5 mg/kg sALP-FcD_{10} into adult WT mice. Circulating $T_{1/2}$ was 34 h, with prolonged retention of the [^{125}I]-labeled sALP-FcD_{10} in bone, with as much as 1 μg/g of bone (wet) weight (Table 1; Fig. 1C). Skeletal levels of the bone-targeted test material seemed stable, because no significant decrease in radiolabeled sALP-FcD_{10} was observed during the experiment. Conversely, no sustained accumulation of sALP-FcD_{10} was observed in muscle, because the amount of radiolabeled enzyme decreased in parallel with sALP-FcD_{10} enzymatic activity in blood (Fig. 1C). Because *Akp2*$^{-/-}$ mice die 12–16 days postnatally and intravenous injection was not feasible in such small animals, PK analysis of sALP-FcD_{10} was planned using intraperitoneal and subcutaneous administration in newborn WT mice. However, intraperitoneal injection proved unreliable because of the high intraabdominal pressure of such young animals, leading to unpredictable losses through the injection site. Instead sub-

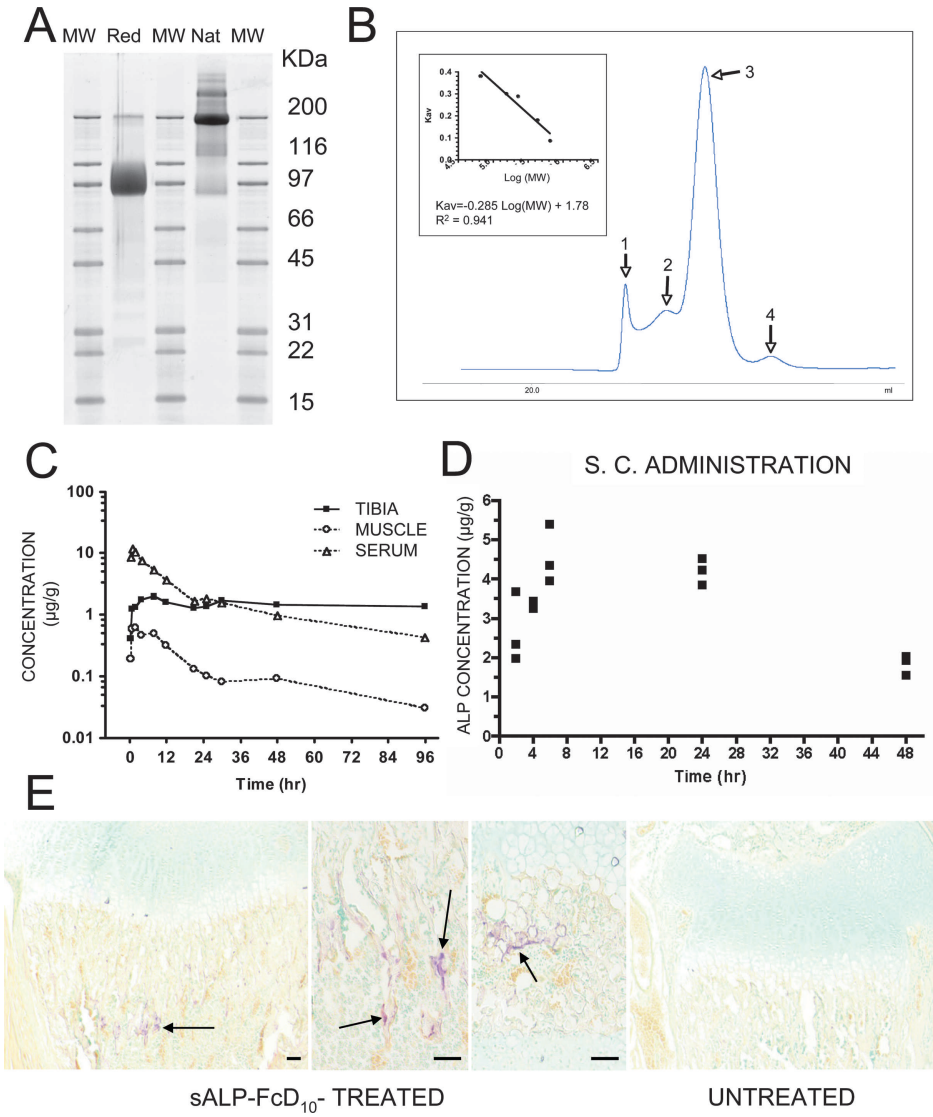

FIG. 1. Purification and properties of recombinant sALP-FcD$_{10}$ and pharmacokinetic and tissue distribution studies. (A) SDS-PAGE of purified sALP-FcD$_{10}$. Protein purified by Protein A-Sepharose affinity chromatography was analyzed by SDS-PAGE and bands were stained with Sypro Ruby. sALP-FcD$_{10}$ migrated as the major species with an apparent molecular mass of ~90,000 Da under reducing conditions (Red) and ~200,000 Da under nonreducing, native conditions (Nat). (B) Characterization of sALP-FcD$_{10}$ by molecular sieve chromatography under nondenaturing conditions. Purified sALP-FcD$_{10}$ protein (2 mg) was resolved on a calibrated column of Sephacryl S-300. The principal form of sALP-FcD$_{10}$ (Peak 3), consisting of 80% of the total material deposited on the column, eluted with a molecular mass of 370,000 Da consistent with a tetrameric structure. When analyzed by SDS-PAGE in the presence of dithiothreitol (DTT), the material in peak 3 migrated with an apparent molecular mass of a monomer. In the absence of DTT, the protein migrated with the mobility of a dimer. (C) Concentrations of radiolabeled sALP-FcD$_{10}$ in serum, tibia, and muscle, expressed as micrograms per gram tissue (wet weight), after a single intravenous bolus of 5 mg/kg in adult WT mice ($n = 3$). (D) Serum concentrations of radiolabeled sALP-FcD$_{10}$ as a function of time after a single subcutaneous injection of 3.7 mg/kg in 1-day-old WT mice ($n = 3$). (E) Histochemical staining for ALP activity in the long bones of sALP-FcD$_{10}$–treated *Akp2*$^{-/-}$ mice. Proximal tibia with EzRT compared with an age-matched untreated *Akp2*$^{-/-}$ mouse. Arrows show areas of ALP activity staining. Bars: 100 μm.

cutaneous injections proved reproducible (Fig. 1D) and were followed by detection of sALP-FcD10 catalytic activity in trabecular bone (Fig. 1E). PK data were used to predict circulating levels of sALP-FcD$_{10}$ after repeated daily subcutaneous injections. Circulating sALP-FcD$_{10}$ would reach steady-state serum concentrations (C) oscillating between C_{min} and C_{max} values of 26.4 and 36.6 μg/ml, respectively, and be achieved after five to six once-daily doses of 10 mg/kg. Prediction validity was tested using five once-daily subcutaneous injections of 10 mg/kg of sALP-FcD$_{10}$. Circulating ALP activity measured 24 h after the last injection (C_{min}) was in good agreement with predicted concentrations. In WT mice, serum TNALP levels measured using these same conditions were found to be 0.58 μg/ml. Thus, we calculated that the subcutaneous injection regimen would achieve steady-state circulating concentrations of sALP-FcD$_{10}$ ~50 times higher than WT TNALP concentrations.

TABLE 1. PHARMACOKINETIC PARAMETERS OF sALP-FcD$_{10}$ IN NEWBORN AND ADULT WT MICE

	Newborn WT		*Adult WT*	
Parameter	*Subcutaneous*	*Intraperitoneal*	*Intraperitoneal*	*Subcutaneous*
$T_{1/2}$ (h)	30.9	19.3	20.0	20.5
T_{max} (h)	6	6	4	NA
C_{max} (mg/liter)	4.6	2.7	10.0	NA
AUC_{inf} (mg/L/h)	257	92	325	362
AUC residual (%)	35	20	20	18
Bioavailability (%)	43	15	89	—

Bioavailability was expressed as percentage of AUC_{inf} in adult WT mice after intravenous injection.

$T_{1/2}$ (h), elimination half-life in hours; C_{max}, maximal concentration; AUC, area under the curve; AUC_{inf}, area under concentration vs. time curve to infinite; NA, not applicable.

Short-term, low-dose (1 and 2 mg/kg/d) treatments with sALP-FcD$_{10}$

The first disease efficacy study using EzRT involved daily subcutaneous injections of sALP-FcD$_{10}$ for 15 days in newborn *Akp2*$^{-/-}$ mice using 1 mg/kg per dose. At this dose, μCT analysis showed no prevention of skeletal disease in the calvarium, and the proximal tibial growth plate (physis) showed excessive widening of the hypertrophic zone consistent with early rickets in both sALP-FcD$_{10}$ and vehicle-injected *Akp2*$^{-/-}$ animals.[21] A daily dose of 2 mg/kg improved the general appearance, body weight, and tail length of treated *Akp2*$^{-/-}$ mice, which also maintained a normal growth rate. BMD of the spine was higher in the treated (238 ± 37 mg/ml) versus untreated (191 ± 13 mg/ml) *Akp2*$^{-/-}$ mice ($p = 0.027$). In the femoral cortical bone, thickness and area tended to be greater in the treated versus untreated mice: 0.11 ± 0.16 versus 0.09 ± 0.04 mm ($p = 0.064$) and 0.39 ± 0.05 versus 0.32 ± 0.01 mm^2 ($p = 0.054$), respectively. Histomorphometry showed no differences in the bone volume fraction (BVF) or trabecular number, but there was greater trabecular thickness. Thus, greater BMD with EzRT was caused by thicker trabeculae. Also, sALP-FcD$_{10}$ preserved BMD and BVF of the proximal trabeculae in the femur and preserved BMD as well as the width and thickness of the frontal and parietal calvarial bones (data not shown).

Short-term and long-term high-dose (8.2 mg/kg/d) treatments with sALP-FcD$_{10}$

Next, we evaluated 15 days of daily subcutaneous injections using the highest dose of sALP-FcD$_{10}$ (8.2 mg/kg). *Akp2*$^{-/-}$ mice were given vehicle ($n = 18$) or treated with sALP-FcD$_{10}$ ($n = 19$). Additionally, there was one non-treated WT mouse per litter ($n = 18$). In all but five treated *Akp2*$^{-/-}$ mice, detectable, but highly variable, levels of sALP-FcD$_{10}$ were found in the plasma (Fig. 2A). EzRT animals had greater body weight than vehicle-treated mice and were indistinguishable from WT mice (Fig. 2B) and had plasma PP_i concentrations in the normal range when the experiment ended.

At completion (day 16), tibia and femur lengths provided additional measures of skeletal benefit for the EzRT mice: for tibias, treated lengths were 12.6 ± 0.7 versus 11.7 ± 1.1 mm for vehicle ($p = 0.014$); for femurs, treated lengths were 9.2 ± 0.4 versus 8.6 ± 0.8 mm for vehicle ($p = 0.027$). Using "blinded" evaluations of Faxitron X-ray images of the feet and rib cages, two degrees of severity of mineralization defects appeared distinguishable in the *Akp2*$^{-/-}$ mice (Fig. 2C). Severely affected mice (severe) had absence of digital bones (phalanges) and secondary ossification centers. Moderately affected mice (moderate) had abnormal secondary ossification centers, but all digital bones were present. WT mice (healthy) had all bony structures present with normal architecture. Radiographic images of the hind limbs were similarly classified as abnormal if evidence of acute or chronic fractures was present, or healthy in the absence of any abnormality (Fig. 2C).

In this short-term experiment, EzRT minimized hypomineralization in the feet documented by the number of *Akp2*$^{-/-}$ mice with severe defects, consisting of five in the untreated group and none in the EzRT group (table in Fig. 2C; $p \leq 0.05$), indicating EzRT decreased the severity of the acquired bone defects. Because severely affected infantile HPP patients often die of undermineralized and fractured ribs incapable of supporting respiration,[4] the thoraces of the mice were also closely examined. EzRT reduced the number of severely dysmorphic rib cages (table in Fig. 2C; $p \leq 0.025$). Similarly, the hind limbs appeared healthy in all treated animals (table in Fig. 2C). χ^2 analysis was significant at $p \leq 0.025$.

We also examined the dentition in vehicle and sALP-FcD$_{10}$-treated mice compared with WT controls (Fig. 3). In *Akp2*$^{-/-}$ mice, the incisor root analog dentin and molar root dentin are particularly sensitive to the lack of TNALP and are only partially mineralized.[38,39] EzRT preserved mineralization at the histological level in both alveolar mandibular bone and in teeth (incisor and molar). There was complete mineralization of all incisor tooth tissues, all molar dentin, and surrounding alveolar bone.

Finally, to assess EzRT for long-term survival and skeletal mineralization, either sALP-FcD$_{10}$ (8.2 mg/kg) or vehicle was subcutaneously administered daily to *Akp2*$^{-/-}$ mice for 52 days. All untreated mice died with a median survival of just 18.5 days (Fig. 4A). In contrast, 75% of EzRT mice (Fig. 4B) lived and showed normal physical activity and a healthy appearance. This preservation of apparent well being with EzRT was accompanied by normal plasma pyridoxal (PL) concentrations (2.9 ± 1.1 μM in *Akp2*$^{-/-}$-treated versus 3.0 ± 1.4 μM in WT mice) and un-

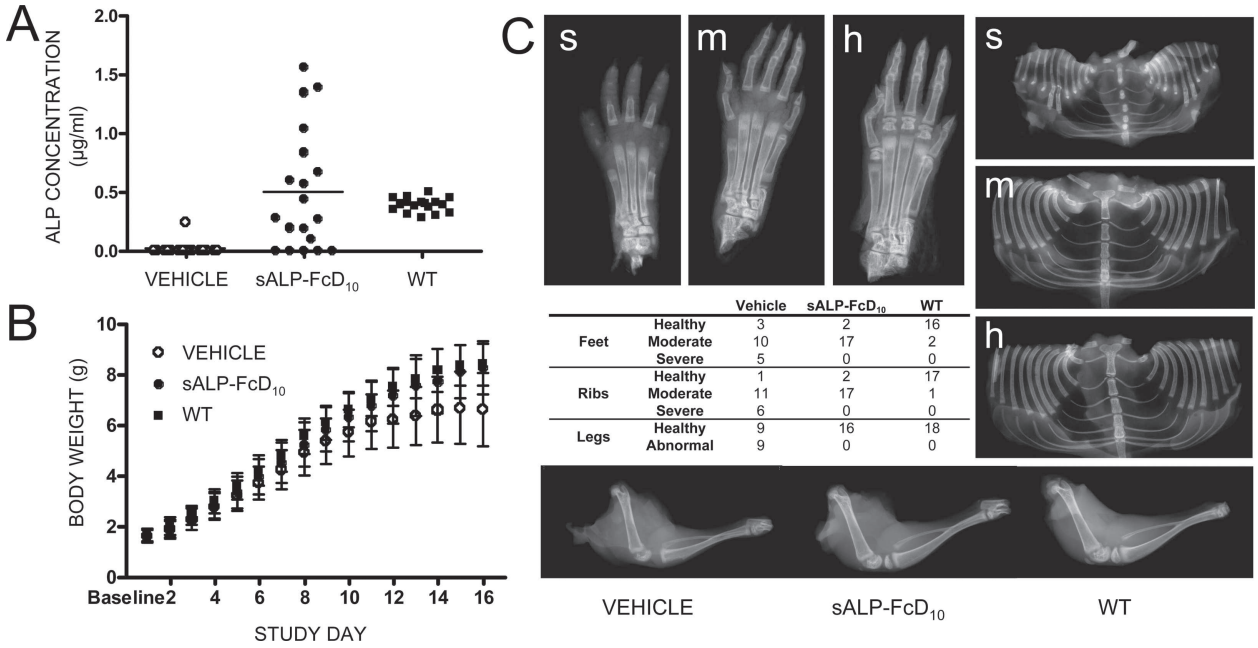

FIG. 2. Short-term, high-dose (8.2 mg/kg) EzRT efficacy studies in *Akp2*$^{-/-}$ mice. (A) Plasma concentrations of ALP activity. (B) Growth curves of *Akp2*$^{-/-}$ mice given vehicle ($n = 18$) or sALP-FcD$_{10}$ ($n = 19$) and nontreated WT mice ($n = 18$). (C) X-ray images of feet, rib cages, and hind limbs of *Akp2*$^{-/-}$ mice (16 days) and a Faxitron image distribution table. Severely (s) affected mice had absence of digital bones (phalanges) and secondary ossification centers. Moderately (m) affected mice had abnormal secondary ossification centers, but all digital bones were present. Healthy (h) WT mice had all bony structures present with normal architecture. Radiographic images of the hind limbs were similarly classified as abnormal if evidence of acute or chronic fractures was present or healthy in the absence of any abnormality.

remarkable calcium concentrations (1.07 ± 0.28 mM in *Akp2*$^{-/-}$-treated versus 1.10 ± 0.24 mM in WT mice). Most plasma ALP concentrations in the EzRT mice were between 1 and 4 μg/ml of sALP-FcD$_{10}$ (Fig. 4C). Radiographs of the hind limbs of 18-day-old untreated *Akp2*$^{-/-}$ mice showed severe skeletal defects, including disappearance of secondary ossification centers, a hallmark of human and murine infantile HPP,[21,40] whereas the skeleton appeared healthy with EzRT at 46 or 52 days (Fig. 4D).

DISCUSSION

Severe forms of HPP (perinatal and infantile) are transmitted as autosomal recessive traits.[6,7] The milder forms (childhood, adult, or odonto-HPP) have either autosomal dominant or autosomal recessive patterns of inheritance.[4,7,8] Two modes of genetic transmission and the many loss-of-function *ALPL* mutations (~200) that can combine with normal or defective *ALPL* alleles largely explain the remarkably variable expressivity that characterizes this inborn error of metabolism.[4] Missense mutations are the most common TNALP defects in HPP and can alter amino acid residues at this dimeric enzyme's active site vicinity, dimer interface, crown domain, amino-terminal arm, or calcium-binding site.[9,10] All such mutations compromise TNALP catalytic activity, although several TNALP active site mutations seem to disrupt hydrolysis of PLP and PP$_i$ differently.[36] Additionally, some TNALP missense, nonsense, frame-shift, or splice site mutations disturb intracellular trafficking of the aberrant protein, further compromising TNALP activity on the surface of osteoblasts and chondrocytes and their MVs where TNALP normally functions as an ectoenzyme.[3]

Diminished hydrolysis of PLP by TNALP explains the pyridoxine-responsive seizures observed in some severely affected HPP patients,[3,4,41] and invariably noted in untreated *Akp2*$^{-/-}$ mice.[11,12,14] Epilepsy occurs because PLP is a co-factor for at least 110 enzymes, including those involved in the biosynthesis of the neurotransmitters γ-aminobutyric acid (GABA), dopamine, and serotonin.[41–43] Dephosphorylation of extracellular PLP to pyridoxal (PL) is a function of ALP, primarily the TNALP isozyme.[44–46] Decreased ecto-TNALP activity in HPP causes increased plasma PLP levels but low PL levels in the most severe cases.[44–46] PL is the vitameric form of vitamin B$_6$ that crosses the plasma membrane for rephosphorylation to PLP within cells. In especially severe HPP, extracellular levels of PL are low, and there seems to be intracellular deficiency of PLP, including in the central nervous system. Seizures from reduced brain levels of GABA in *Akp2*$^{-/-}$ mice are caused by glutamic acid decarboxylase dysfunction secondary to the intracellular PLP deficiency.[11,41]

In HPP patients, diminished hydrolysis of PP$_i$ explains the impaired skeletal mineralization leading to rickets or osteomalacia,[3,4] which is recapitulated as acquired rickets in *Akp2*$^{-/-}$ mice.[19,21–24,40] TNALP controls extracellular concentrations of PP$_i$, an inhibitor of hydroxyapatite crystal nucleation and growth,[4] and thus regulates skeletal min-

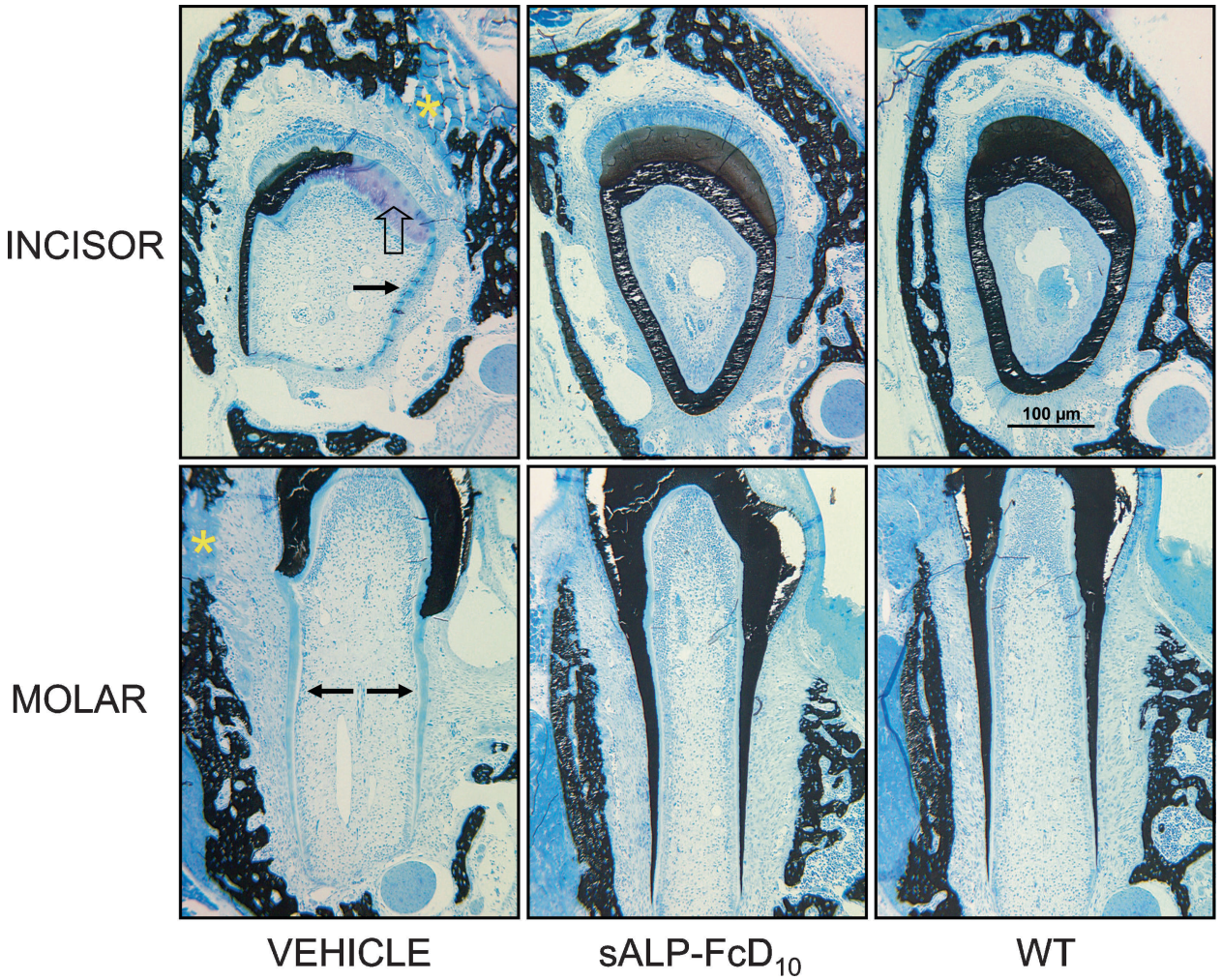

FIG. 3. Preservation of *Akp2*$^{-/-}$ tooth and alveolar bone architecture by EzRT. Mandibles from 16-day-old mice (WT, sALP-FcD$_{10}$-treated *Akp2*$^{-/-}$, and vehicle-injected *Akp2*$^{-/-}$) were cut into segments containing the first molar, the underlying incisor, and the surrounding alveolar bone. Tooth type and treatment are as indicated. Note the incisor from a vehicle-injected *Akp2*$^{-/-}$ mouse showing only partial mineralization of the dentin. Extensive regions of unmineralized crown analog dentin (open arrow) and unmineralized root analog dentin (arrow) are present. Likewise, the surrounding alveolar bone also shows regions of unmineralized bone matrix (asterisk). sALP-FcD$_{10}$ treatment of *Akp2*$^{-/-}$ mice preserves complete mineralization of all incisor tooth tissues and the surrounding alveolar bone, such that no mineralization differences are seen between the incisor teeth and bone of the EzRT mice compared with WT mice. Note also the molar from a vehicle-injected *Akp2*$^{-/-}$ mouse showing only partial mineralization of the dentin. Extensive regions of unmineralized root dentin (arrows) are present, as are regions of unmineralized alveolar bone matrix (asterisk). EzRT maintains complete mineralization of all molar dentin as well as the surrounding alveolar bone such that no mineralization differences are seen between the molar teeth and bone of the treated mice compared with WT mice. Magnification bar = 100 μm. All images were taken at the same magnification.

eralization.[3,10] TNALP is especially abundant on the cell surface of osteoblasts and chondrocytes, including on their shed MVs.[16,17] Beginning with Robison's discovery of ALP,[47] some have hypothesized that TNALP in bone also generates P_i needed for hydroxyapatite crystal formation.[47–49] In addition, GPI-anchored TNALP may control the quality of deposited mineral, at least in vitro.[50] Clearly, however, TNALP hydrolyzes PP_i to facilitate both mineral precipitation and hydroxyapatite crystal growth.[49,51,52] Recent studies using *Akp2*$^{-/-}$ mice confirm a major physiologic role for TNALP in restricting the size of the extracellular PP_i pool.[21–24]

Although the biochemical mechanism that leads to the skeletal and dental defects of HPP is now generally understood, there is no established medical treatment.[4] Uncontrolled trials of EzRT for a few patients, especially those with infantile HPP, using intravenous infusions of TNALP-rich plasma obtained by plasmapheresis from individuals with Paget's bone disease,[25,26] have shown no consistent radiographic evidence for arrest of progressive skeletal demineralization or improvement in rachitic defects. This is so despite transient correction or overcorrection of the hypophosphatasemia. Similarly, intravenous infusions of purified human liver TNALP[27] or purified placental ALP[28] were without significant benefit. Sequential radiographic studies showed no clinically important correction of bone

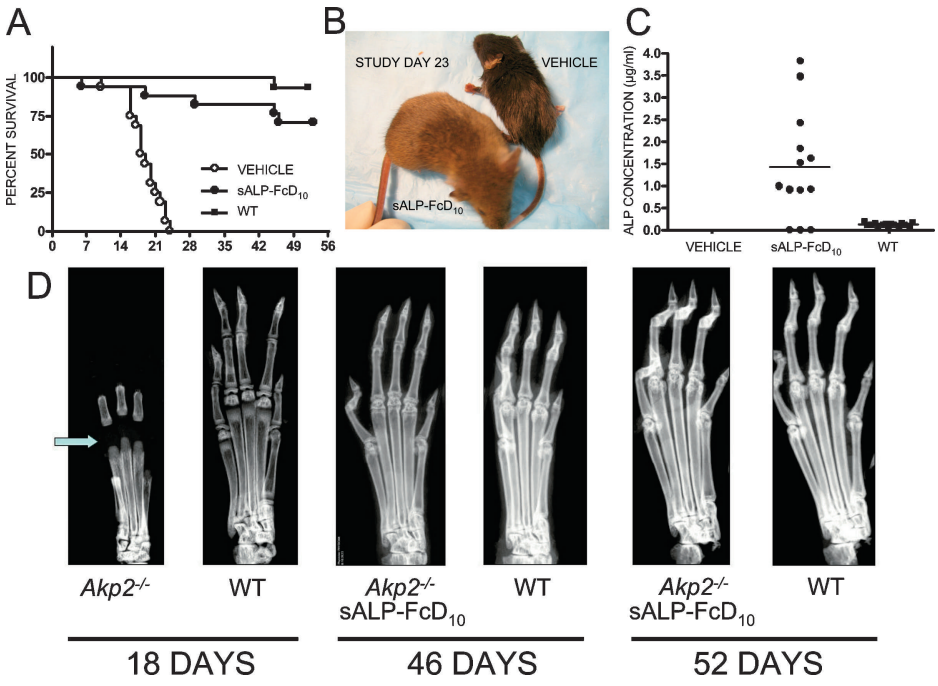

FIG. 4. Long-term (52 days), high-dose (8.2 mg/kg) EzRT efficacy studies in *Akp2*$^{-/-}$ mice. (A) Long-term survival of EzRT mice contrasts with precipitous, early demise of the vehicle-treated group. (B) Normal appearance of an EzRT mouse compared with a stunted, vehicle-treated animal. (C) Plasma ALP concentration in untreated and treated *Akp2*$^{-/-}$ mice and WT controls. (D) X-ray image of the hind paw of an 18-day-old untreated *Akp2*$^{-/-}$ mouse showing absence of secondary ossification centers (arrow). In contrast, note the normal appearances of the hind paws of 46- and 52-day-old *Akp2*$^{-/-}$ mice receiving EzRT.

mineralization. Such therapy failures could be explained by relatively brief periods of treatment, insufficient steady-state circulating concentrations of ALP, or inability of the administered soluble ALP to reach and be retained at sites of skeletal mineralization.[3,4]

We hypothesized that a bone-targeted form of TNALP administered from birth to *Akp2*$^{-/-}$ mice would mitigate the skeletal phenotype of HPP. We document here that this approach for EzRT using sALP-FcD$_{10}$ prevents characteristic rickets and lethal epilepsy while sustaining their growth rates, appearance, and apparent well being.

We created a soluble form of human TNALP shown to have a high affinity for hydroxyapatite crystals caused by the presence of a repetitive C-terminal extension of 10 Asp residues (D$_{10}$). This type of construct has been shown[37] to display high affinity for bone tissue in vitro, and in our study sALP-FcD$_{10}$ bound 32-fold better to hydroxyapatite than did a nontargeted ALP (i.e., native kidney TNALP). Furthermore, we showed that the intervening IgG Fc sequence between the C terminus of the TNALP ectodomain and the D$_{10}$ sequence of sALP-FcD$_{10}$ enables rapid purification of the chimeric protein by affinity chromatography on Protein-A Sepharose. We stably transfected the cDNA encoding the chimeric protein into CHO cells and further amplified the number of integrated cDNA copies using methotrexate. Using this approach, we identified a highly productive CHO clone enabling the biosynthesis and purification of sALP-FcD$_{10}$ from the culture medium, reaching concentrations of up to 3.5 mg/liter after 3 days of culture.

TNALP monomers associate into enzymatically active homodimers linked by noncovalent bonds, but when separated, the subunits have no enzymatic activity.[10] When analyzed by molecular sieve chromatography under nondenaturing conditions, recombinant sALP-FcD$_{10}$ appears to consist primarily of homotetramers. Our data suggest that these tetramers are formed by noncovalent association of two sALP-FcD$_{10}$ dimers that are disulfide-linked at their Fc segments. For such dimers, steric constraints imposed by the two disulfide bridges in the hinge region of the Fc sequence probably prevent noncovalent association of the two sALP domains into a functional enzymatically active unit. Because the tetramers are enzymatically active, it is likely that they are formed by the association of two sALP moieties carried by two different disulfide bonded Fc dimers. A similar tetrameric structure of TNALP has been hypothesized for the native GPI-anchored form in the cell membrane and has been proposed to constitute the fully functional enzymatic unit.[53]

With a reliable source of recombinant enzyme, we were able to test our EzRT strategy using the *Akp2*$^{-/-}$ mouse as a model of infantile HPP. Pharmacokinetics and the tissue distribution of sALP-FcD$_{10}$ in adult WT mice indicated a circulating half-life of 34 h and skeletal accumulation of radiolabeled sALP-FcD$_{10}$ up to a level of 1 μg/g of bone (wet weight). This circulating half-life resembles experience from the unsuccessful clinical trials for EzRT.[25–28] Our initial *Akp2*$^{-/-}$ mouse studies showed that subcutaneous injection was a suitable means of enzyme administration for newborn mice. Steady-state circulating concentrations up to 50-fold higher than in WT mice would be obtained after five to six once-daily doses of 10 mg/kg of sALP-FcD$_{10}$. To conserve available sALP-FcD$_{10}$, short-term feasibility studies used smaller doses of 1, 2, and 8.2 mg/kg. The 1-mg/kg dose was insufficient to prevent the HPP bone phenotype assessed by μCT analysis. A dose of 2 mg/kg, however, was adequate to maintain a healthy growth curve and apparent well being for the treated mice and to maintain BMD of the calvarium, femur, and spine. Ultimately, both short-term and long-term treatment with the highest dose (8.2 mg/kg/d) preserved the life span of the *Akp2*$^{-/-}$ mice and pre-

vented epileptic seizures. Normal plasma PP_i and PL concentrations in the EzRT mice confirmed preservation of both major biochemical pathways disrupted by absence of TNALP activity. At this higher dose, complete maintenance of skeletal and dental architecture was observed after 15 days with a daily subcutaneous injection regimen, and bone lesions were not seen after 52 days of treatment.

Patients with perinatal or infantile HPP,[3] as well as TNALP knockout mice,[13] can manifest hypercalcemia, which seems to result from decreased uptake of mineral by the skeleton.[4] There may also be a component of mineral loss from bone when sequential radiographs show progressive skeletal demineralization heralding a lethal outcome for severely affected babies and in the knockout mice that develop skeletal disease early in life. It is not clear why renal and/or intestinal function fails to compensate for the hypercalcemia.[4] Circulating PTH and 1,25-dihydroxyvitamin D levels are often physiologically suppressed, yet the gut seems to absorb enough calcium to contribute to the hypercalcemia and hypercalciuria.[30] Circulating P_i levels tend to be high-normal or elevated in HPP patients,[4] yet do not correct the hypercalcemia from an increased calcium-phosphate product or by suppressing 1,25-dihydroxyvitamin D biosynthesis. Normal plasma calcium concentrations with EzRT in *Akp2*$^{-/-}$ mice are therefore consistent with their properly growing skeleton.[3]

Our findings revealed that sustained delivery of bone-targeted TNALP can prevent the sequelae of infantile HPP recapitulated in *Akp2*$^{-/-}$ mice. These observations represent the first demonstration of successful EzRT to prevent a primary skeletal disease of genetic origin in a mouse model and are a foundation for future EzRT trials for HPP patients.

ACKNOWLEDGMENTS

The authors thank Kristen Johnson, PhD, for help in establishing the plasma PP_i assay in our laboratories. We acknowledge the expert technical contributions and dedication from Enobia employees Eric Bouchard, Annie Salesse, Claire Vézina, Caroline Meilleur, Johanne Pion, Mathieu Brossard, Julie Guimond, Éric Leblanc, Line Lespérance, and Jacqueline Yep. This work was supported by Grants DE12889 and AR47908 from the National Institutes of Health, from Enobia Pharma, and from the Shriners Hospitals for Children and used the facilities of the Hospital for Special Surgery's Core Center for Musculoskeletal Repair and Regeneration, supported by NIH Grant AR46121.

REFERENCES

1. Rathbun JC 1948 Hypophosphatasia, a new developmental anomaly. Am J Dis Child **75:**822–831.
2. Fraser D 1957 Hypophosphatasia. Am J Med **22:**730–746.
3. Whyte MP 1994 Hypophosphatasia and the role of alkaline phosphatase in skeletal mineralization. Endocr Rev **15:**439–461.
4. Whyte MP 2001 Hypophosphatasia. In: Scriver CR, Beaudet AL, Sly WS, Valle D, Childs B, Kinzler KW (eds.) The Metabolic and Molecular Bases of Inherited Disease. McGraw-Hill, New York, NY, USA, pp. 5313–5329.
5. Greenberg CR, Taylor CL, Haworth JC, Seargeant LE, Philipps S, Triggs-Raine B, Chodirker BN 1993 A homoallelic Gly317→Asp mutation in ALPL causes the perinatal (lethal) form of hypophosphatasia in Canadian mennonites. Genomics **17:**215–217.
6. Weiss MJ, Cole DE, Ray K, Whyte MP, Lafferty MA, Mulivor RA, Harris H 1988 A missense mutation in the human liver/bone/kidney alkaline phosphatase gene causing a lethal form of hypophosphatasia. Proc Natl Acad Sci USA **85:**7666–7669.
7. Henthorn PS, Raducha M, Fedde KN, Lafferty MA, Whyte MP 1992 Different missense mutations at the tissue-nonspecific alkaline phosphatase gene locus in autosomal recessively inherited forms of mild and severe hypophosphatasia. Proc Natl Acad Sci USA **89:**9924–9928.
8. Henthorn PS, Whyte MP 1992 Missense mutations of the tissue-nonspecific alkaline phosphatase gene in hypophosphatasia. Clin Chem **38:**2501–2505.
9. Zurutuza L, Muller F, Gibrat JF, Taillandier A, Simon-Bouy B, Serre JL, Mornet E 1999 Correlations of genotype and phenotype in hypophosphatasia. Hum Mol Genet **8:**1039–1046.
10. Millán JL 2006 Mammalian Alkaline Phosphatases. From Biology to Applications in Medicine and Biotechnology. Wiley-VCH Verlag, Weinheim, Germany.
11. Waymire KG, Mahuren JD, Jaje JM, Guilarte TR, Coburn SP, MacGregor GR 1995 Mice lacking tissue non-specific alkaline phosphatase die from seizures due to defective metabolism of vitamin B-6. Nat Genet **11:**45–51.
12. Narisawa S, Fröhlander N, Millán JL 1997 Inactivation of two mouse alkaline phosphatase genes and establishment of a model of infantile hypophosphatasia. Dev Dyn **208:**432–446.
13. Fedde KN, Blair L, Silverstein J, Coburn SP, Ryan LM, Weinstein RS, Waymire K, Narisawa S, Millán JL, MacGregor GR, Whyte MP 1999 Alkaline phosphatase knock-out mice recapitulate the metabolic and skeletal defects of infantile hypophosphatasia. J Bone Miner Res **14:**2015–2026.
14. Narisawa S, Wennberg C, Millán JL 2001 Abnormal vitamin B6 metabolism in alkaline phosphatase knockout mice causes multiple abnormalities, but not the impaired bone mineralization. J Pathol **193:**125–133.
15. Ali SY, Sajdera SW, Anderson HC 1970 Isolation and characterization of calcifying matrix vesicles from epiphyseal cartilage. Proc Natl Acad Sci USA **67:**1513–1520.
16. Bernard GW 1978 Ultrastructural localization of alkaline phosphatase in initial intramembranous osteogenesis. Clin Orthop **135:**218–225.
17. Morris DC, Masuhara K, Takaoka K, Ono K, Anderson HC 1992 Immunolocalization of alkaline phosphatase in osteoblasts and matrix vesicles of human fetal bone. Bone Miner **19:**287–298.
18. Anderson HC, Hsu HH, Morris DC, Fedde KN, Whyte MP 1997 Matrix vesicles in osteomalacic hypophosphatasia bone contain apatite-like mineral crystals. Am J Pathol **151:**1555–1561.
19. Anderson HC, Sipe JE, Hessle L, Dhamyamraju R, Atti E, Camacho NP, Millán JL 2004 Impaired calcification around matrix vesicles of growth plate and bone in alkaline phosphatase-deficient mice. Am J Pathol **164:**841–847.
20. Meyer JL 1984 Can biological calcification occur in the presence of pyrophosphate? Arch Biochem Biophys **231:**1–8.
21. Hessle L, Johnson KA, Anderson HC, Narisawa S, Sali A, Goding JW, Terkeltaub R, Millán JL 2002 Tissue-nonspecific alkaline phosphatase and plasma cell membrane glycoprotein-1 are central antagonistic regulators of bone mineralization. Proc Natl Acad Sci USA **99:**9445–9449.
22. Harmey D, Hessle L, Narisawa S, Johnson KA, Terkeltaub R, Millán JL 2004 Concerted regulation of inorganic pyrophosphate and osteopontin by *Akp2, Enpp1*, and *Ank*: An integrated model of the pathogenesis of mineralization disorders. Am J Pathol **164:**1199–1209.
23. Murshed M, Harmey D, Millán JL, McKee MD, Karsenty G 2005 Unique coexpression in osteoblasts of broadly expressed

genes accounts for the spatial restriction of ECM mineralization to bone. Genes Dev **19:**1093–1104.
24. Harmey D, Johnson KA, Zelken J, Camacho NP, Hoylaerts MF, Noda M, Terkeltaub R, Millán JL 2006 Elevated skeletal osteopontin levels contribute to the hypophosphatasia phenotype in *Akp2*$^{-/-}$ mice. J Bone Miner Res **21:**1377–1386.
25. Whyte MP, Valdes R Jr, Ryan LM, McAlister WH 1982 Infantile hypophosphatasia: Enzyme replacement therapy by intravenous infusion of alkaline phosphatase-rich plasma from patients with Paget bone disease. J Pediatr **101:**379–386.
26. Whyte MP, McAlister WH, Patton LS, Magill HL, Fallon MD, Lorentz WB Jr, Herrod HG 1984 Enzyme replacement therapy for infantile hypophosphatasia attempted by intravenous infusions of alkaline phosphatase-rich Paget plasma: Results in three additional patients. J Pediatr **105:**926–933.
27. Weninger M, Stinson RA, Plenk H Jr, Böck P, Pollak A 1989 Biochemical and morphological effects of human hepatic alkaline phosphatase in a neonate with hypophosphatasia. Acta Paediatr Scand Suppl **360:**154–160.
28. Whyte MP, Habib D, Coburn SP, Tecklenburg F, Ryan L, Fedde KN, Stinson RA 1992 Failure of hyperphosphatasemia by intravenous infusion of purified placental alkaline phosphatase (ALP) to correct severe hypophosphatasia: Evidence against a role for circulating ALP in skeletal mineralization. J Bone Miner Res **7:**S2;S155.
29. Whyte MP, Kurtzberg J, McAlister WH, Mumm S, Podgornik MN, Coburn SP, Ryan LM, Miller CR, Gottesman GS, Smith AK, Douville J, Waters-Pick B, Armstrong RD, Martin PL 2003 Marrow cell transplantation for infantile hypophosphatasia. J Bone Miner Res **18:**624–636.
30. Cahill RA, Wenkert D, Perlman SA, Steele A, Coburn SP, McAlister WH, Mumm S, Whyte MP 2007 Infantile hypophosphatasia: Transplantation therapy trial using bone fragments and cultured osteoblasts. J Clin Endocrinol Metab **92:**2923–2930.
31. Urlaub G, Käs E, Carothers AM, Chasin LA 1983 Deletion of the diploid dihydrofolate reductase locus from cultured mammalian cells. Cell **33:**405–412.
32. Johnson K, Moffa A, Chen Y, Pritzker K, Goding J, Terkeltaub R 1999 Matrix vesicle plasma cell membrane glycoprotein-1 regulates mineralization by murine osteoblastic MC3T3 cells. J Bone Miner Res **14:**883–892.
33. Sharma SK, Dakshinamurti K 1992 Determination of vitamin B6 vitamers and pyridoxic acid in biological samples. J Chromatogr A **578:**45–51.
34. Baginski ES, Marie SS, Clark WL, Zak B 1973 Direct microdetermination of serum calcium. Clin Chim Acta **46:**49–54.
35. Narisawa S, Hasegawa H, Watanabe K, Millán JL 1994 Stage-specific expression of alkaline phosphatase during neural development in the mouse. Dev Dyn **201:**227–235.
36. Di Mauro S, Manes T, Hessle H, Kozlenkov A, Pizauro JM, Hoylaerts MF, Millán JL 2002 Kinetic characterization of hypophosphatasia mutations with physiological substrates. J Bone Miner Res **17:**1383–1391.
37. Nishioka T, Tomatsu S, Gutierrez MA, Miyamoto K, Trandafirescu GG, Lopez PL, Grubb JH, Kanai R, Kobayashi H, Yamaguchi S, Gottesman GS, Cahill R, Noguchi A, Sly WS 2006 Enhancement of drug delivery to bone: Characterization of human tissue-nonspecific alkaline phosphatase tagged with an acidic oligopeptide. Mol Genet Metab **88:**244–255.
38. Beertsen W, Van den Bos T, Everts V 1999 Root development in mice lacking functional tissue non-specific alkaline phosphatase gene: Inhibition of acellular cementum formation. J Dent Res **78:**1221–1229.
39. Van den Bos T, Handoko G, Niehof A, Ryan LM, Coburn SP, Whyte MP, Beertsen W 2005 Cementum and dentin in hypophosphatasia. J Dent Res **84:**1021–1025.
40. Anderson HC, Harmey D, Camacho NP, Garimella R, Sipe JB, Tague S, Bi X, Johnson K, Terkeltaub R, Millán JL 2005 Sustained osteomalacia of long bones despite major improvement in other hypophosphatasia-related mineral deficits in tissue nonspecific alkaline phosphatase/nucleotide pyrophosphatase phosphodiesterase 1 double deficient mice. Am J Pathol **166:**1711–1720.
41. Baumgartner-Sigl S, Haberlandt E, Mumm S, Scholl-Bürgi S, Sergi C, Ryan L, Ericson KL, Whyte MP, Högler W 2007 Pyridoxine-responsive seizures as the first symptom of infantile hypophosphatasia caused by two novel missense mutations (c.677T>C, p.M226T; c.1112C>T, p.T371I) of the tissue-nonspecific alkaline phosphatase gene. Bone **40:**1655–1661.
42. Coburn SP 1996 Modeling vitamin B6 metabolism. Adv Food Nutr Res **40:**107–132.
43. Jansonius JN 1998 Structure, evolution and action of vitamin B6-dependent enzymes. Curr Opin Struct Biol **8:**759–769.
44. Whyte MP, Mahuren JD, Vrabel LA, Coburn SP 1985 Markedly increased circulating pyridoxal-5′-phosphate levels in hypophosphatasia. Alkaline phosphatase acts in vitamin B6 metabolism. J Clin Invest **76:**752–756.
45. Whyte MP, Mahuren JD, Fedde KN, Cole FS, McCabe ER, Coburn SP 1988 Perinatal hypophosphatasia: Tissue levels of vitamin B6 are unremarkable despite markedly increased circulating concentrations of pyridoxal-5′-phosphate. Evidence for an ectoenzyme role for tissue-nonspecific alkaline phosphatase. J Clin Invest **81:**1234–1239.
46. Whyte MP, Landt M, Ryan LM, Mulivor RA, Henthorn PS, Fedde KN, Mahuren JD, Coburn SP 1995 Alkaline phosphatase: Placental and tissue-nonspecific isoenzymes hydrolyze phosphoethanolamine, inorganic pyrophosphate, and pyridoxal 5′-phosphate. Substrate accumulation in carriers of hypophosphatasia corrects during pregnancy. J Clin Invest **95:**1440–1445.
47. Robison R 1923 The possible significance of hexosephosphoric esters in ossification. Biochem J **17:**286–293.
48. Majeska RJ, Wuthier RE 1975 Studies on matrix vesicles isolated from chick epiphyseal cartilage. Association of pyrophosphatase and ATPase activities with alkaline phosphatase. Biochim Biophys Acta **391:**51–60.
49. McComb RB, Bowers GN Jr, Posen S 1979 Alkaline Phosphatase. Plenum Press, New York, NY, USA.
50. Harrison G, Shapiro IM, Golub EE 1995 The phosphatidylinositol-glycolipid anchor on alkaline phosphatase facilitates mineralization initiation in vitro. J Bone Miner Res **10:**568–573.
51. Moss DW, Eaton RH, Smith JK, Whitby LG 1967 Association of inorganic-pyrophosphatase activity with human alkaline-phosphatase preparations. Biochem J **102:**53–57.
52. Rezende LA, Ciancaglini P, Pizauro JM, Leone FA 1998 Inorganic pyrophosphate-phosphohydrolytic activity associated with rat osseous plate alkaline phosphatase. Cell Mol Biol (Noisy-le-grand) **44:**293–302.
53. Hawrylak K, Stinson RA 1988 The solubilization of tetrameric alkaline phosphatase from human liver and its conversion into various forms by phosphatidylinositol phospholipase C or proteolysis. J Biol Chem **263:**14368–14373.

Address reprint requests to:
José Luis Millán, PhD
Burnham Institute for Medical Research
10901 North Torrey Pines Road
La Jolla, CA 92037, USA
E-mail: millan@burnham.org

Received in original form September 7, 2007; revised form December 5, 2007; accepted December 14, 2007.